Relativistic continuum quasiparticle random-phase approximation in spherical nuclei

I. Daoutidis[1] and P. Ring[2]
[1]*Institut d'Astronomie et d'Astrophysique, Université Libre de Bruxelles, B-1050 Bruxelles, Belgium*
[2]*Physik-Department der Technischen Universität München, D-85748 Garching, Germany*
(Received 11 January 2011; published 5 April 2011)

We have calculated the strength distributions of the dipole response in spherical nuclei, ranging all over the periodic table. The calculations were performed within two microscopic models: the discretized quasiparticle random-phase approximation and the continuum quasiparticle random-phase approximation, which takes into account the coupling of the single-particle continuum in an exact way. Pairing correlations are treated with the BCS model. In the calculations, two density functionals were used, namely, the PC-F1 and the DD-PC1. Both are based on relativistic point-coupling Lagrangians. It is explicitly shown that this model is capable of reproducing the giant- as well as the pygmy-dipole resonance for open-shell nuclei in a high level of quantitative agreement with the available experimental observations.

DOI: 10.1103/PhysRevC.83.044303 PACS number(s): 24.30.Cz, 24.10.Jv, 21.60.Jz, 21.10.−k

I. INTRODUCTION

The investigation of the isovector giant-dipole resonances (IVGDRs) is one of the fundamental problems in nuclear physics and astrophysics. These collective resonances can be studied experimentally by photon scattering (γ,γ') or photodissociation (γ,n) processes, as well as by means of nuclear-resonance fluorescence using linearly polarized and unpolarized bremsstrahlung [1]. Theoretical investigations are based mainly on self-consistent microscopic approaches, such as the random-phase approximation (RPA) or the quasiparticle RPA (QRPA), which is a straightforward generalization of the RPA including pairing correlations.

In solving the RPA equations, one should take into account all the particle-hole pairs that contribute to the excitation. The most common but computationally expensive way of doing this is by discretizing the basis and introducing a truncation (cutoff) parameter for the otherwise infinite configuration space. However, despite the fact that these models, in principle, enable one to reproduce experimental mean energies and total strengths of the giant resonances, they fail to describe their finite structure. One of the reasons is that the RPA and the QRPA do not provide a mechanism that produces the escape width $\Gamma^{\uparrow}$, which gives a considerable contribution to the total width of the giant-multipole resonances. In addition, the space truncation which is required by the numerical calculations leads to model deficiencies, such as deviations of the resonance energy or mixing of spurious states coming from symmetry breaking with the physical states.

There is the alternative method of the continuum RPA [2] which avoids a basis truncation by treating the single-particle continuum explicitly. As a consequence, the entire configuration space is included effectively, without the need of energy cutoffs. Despite the fact that the continuum RPA (CRPA) is proven to be a more complete and numerically faster approach than any other RPA method available, it has been applied in the past mostly in the nonrelativistic framework [2–18]. Applications of the relativistic continuum RPA have been restricted to cases without pairing correlations, i.e., to doubly magic nuclei [19–22]. Recently, a CRPA approach based on relativistic point-coupling models has been developed to study giant-multipole resonances for spherical doubly magic nuclei in the entire periodic table [23].

Apart from the well-studied giant-dipole resonance (GDR), the pygmy resonance (IVPR) which appears as a soft low-lying mode in the dipole spectrum of neutron-rich nuclei has still a lot to reveal [24]. A concept that attracts most of the attention is the picture of an oscillation of the excess neutrons against the isospin-saturated proton-neutron core. Furthermore, low-lying $E1$ strength in unstable nuclei is currently also discussed in the context of the astrophysical r-process nucleosynthesis [25], since it can affect the neutron capture rates, which are important quantities in the determination of the r-process path. The main difficulty in the study of this mode is due to the fact that its excitation energy is very close to and sometimes even below the particle emission threshold, hindering in that way its experimental identification, especially when a photodissociation (γ,n) process is used.

In the present paper, we investigate theoretically the dipole strength distribution for several even-even nuclei all over the nuclear chart. The calculations are performed within the framework of continuum QRPA (CQRPA) as well as of conventional QRPA, where the continuum is discretized. Pairing correlations in open-shell nuclei are treated within the BCS model. Introducing finite occupation probabilities for the single-particle spectrum of the relativistic mean field (RMF) theory is a very successful scheme for treating pp correlations in these nuclei. In addition, dynamical pairing is applied on the RPA level with an additional pp term in the effective interaction. In this way, the approach is fully self-consistent and spurious states due to restoration of symmetries, such as translation and particle-number invariance, are properly separated from the rest of the spectrum.

It has to be emphasized, however, that the BCS model faces serious problems in nuclei with a large neutron excess in the neighborhood of the drip line where the Fermi level is close to the continuum. In these cases, one has to use the full Hartree-Fock-Bogoliubov [26,27] or relativistic-Hartree-Bogoliubov (RHB) [28–30] theory which treats pairing correlations in a

more consistent way. But, since we concentrate here on stable nuclei far from the drip lines, BCS is a suitable model.

The paper is organized as follows. In Sec. II, we briefly describe the continuum QRPA based on relativistic point-coupling Lagrangians. In Sec III, we perform calculations on isovector dipole and pygmy resonances for several Sn isotopes and compare the results using the various successful parameter sets. Conclusions are drawn in Sec. IV.

II. THE POINT-COUPLING MODEL

As in all relativistic models, the nucleons are described as pointlike Dirac particles. In contrast to the Walecka model [31], however, where these particles interact by the exchange of effective mesons with finite mass, point-coupling models [32,33] neglect mesonic degrees of freedom and consider only interactions with zero range. In principle, these models are similar to the Nambu–Jona-Lasinio model [34] used extensively in hadron physics. There is, however, an important difference: In order to obtain a satisfactory description of the nuclear surface properties, one also needs gradient terms in the Lagrangian simulating a finite range of the interaction. In this work, we use two different point-coupling Lagrangians: the set PC-F1 introduced by Bürvenich *et al.* in Ref. [35] and the more recent set DD-PC1 introduced by Nikšić *et al.* [36]. In both cases, the Lagrangian is represented in terms of the nucleon scalar (S), vector (V), and isovector vector (TV) fields:

$$\mathcal{L} = \bar{\psi}(i\gamma\cdot\partial - m)\psi - \sum_i \frac{1}{2}\alpha_i[\rho](\bar{\psi}\hat{\Gamma}_i\psi)(\bar{\psi}\hat{\Gamma}_i\psi) - \frac{1}{2}\delta_i(\partial_\nu\bar{\psi}\hat{\Gamma}_i\psi)(\partial^\nu\bar{\psi}\hat{\Gamma}_i\psi) - e^2(\bar{\psi}\hat{\Gamma}_C\psi)(\bar{\psi}\hat{\Gamma}_C\psi), \quad (1)$$

where the Dirac vertices $\hat{\Gamma}_i$ $(i = \mathrm{S},\ \mathrm{V},\ \mathrm{TV})$ and the electromagnetic vertex $\hat{\Gamma}_C$ have the explicit form

$$\hat{\Gamma}_\mathrm{S} = 1, \quad \hat{\Gamma}_\mathrm{V} = \gamma_\mu, \quad \hat{\Gamma}_\mathrm{TV} = \gamma_\mu\vec{\tau}, \quad \hat{\Gamma}_C = \gamma_\mu\frac{(1-\tau_3)}{2}. \quad (2)$$

The coupling constants α_i depend on the density, and this density dependence is different for the two forces. While, for PC-F1, each $\alpha_i[\rho_i]$ in the various spin-isospin channels depends on the corresponding local densities ρ_i, for DD-PC1, all the couplings $\alpha_i[\rho]$ depend on the baryon density $\rho = \rho_\mathrm{V}$ alone. In particular, one has

$$\alpha_i[\rho] = \begin{cases} a_i + b_i\rho_i + c_i\rho_i^2 & \text{for} \quad \mathrm{PC-F1}, \\ a_i + (b_i + c_i x)e^{-d_i x} & \text{for} \quad \mathrm{DD-PC1}, \end{cases} \quad (3)$$

where $x = \rho/\rho_\mathrm{sat}$ denotes the nucleon density in units of the saturation density in symmetric nuclear matter.

In addition, DD-PC1, unlike its predecessors, has not been adjusted to spherical nuclei, but to *ab initio* calculations together with nuclear matter data and to a large set of axially deformed nuclei. The two sets are listed in Table I, and they have been tested in the calculation of many ground-state properties of spherical and deformed nuclei all over the periodic table [37]. The results are very well comparable with reasonable effective meson-exchange interactions [38–40].

TABLE I. Coupling constants for the density functionals PC-F1 and DD-PC1 resulting from the fitting procedures in Ref. [35] and Ref. [36], respectively. The parameters d_i of DD-PC1 are dimensionless.

	PC-F1	DD-PC1
a_S	$-14.935\,894$ fm^{-2}	-10.0462 fm^{-2}
b_S	$22.994\,736$ fm^{-5}	-9.1504 fm^{-2}
c_S	$-66.769\,116$ fm^{-8}	-6.4273 fm^{-2}
d_S		1.3724
δ_S	$-0.634\,576$ fm^{-2}	-0.8149 fm^{-4}
a_V	$10.098\,025$ fm^{-2}	5.9195 fm^{-2}
b_V	0.0	8.8637 fm^{-2}
c_V	$-8.917\,323$ fm^{-8}	0.0
d_V		0.6584
δ_V	-0.180746 fm^{-2}	0.0
a_TV	$1.350\,268$ fm^{-2}	0.0
b_TV	0.0	1.8360 fm^{-2}
c_TV	0.0	0.0
d_TV		0.6403
δ_TV	$-0.063\,680$ fm^{-2}	0.0

However, the success of a particular interaction relies on the ability to reproduce, apart from the static properties of a broad range of nuclei, also their dynamical properties, as, for instance, the properties of collective multipole resonances via the microscopic RPA approaches, which we will discuss in the next section.

A. Linear response theory

If a nucleus is exposed to an external field, such as in the photoabsorption process, the strength function

$$S(\omega) = -\frac{1}{\pi}\mathrm{Im}\sum_{\alpha\beta} F_\alpha^* R_{\alpha\beta}(\omega)F_\beta \quad (4)$$

measures the change of the nuclear density due to the influence of this field. TheGreek indices α and β indicate the various degrees of freedom of a nucleus (r, L, S, T), while F is the operator of the external field.

If we consider only small amplitude variations of the density taking into account only one-particle-one-hole $(1ph)$ excitations, the response function $R(\omega)$ can be deduced from the linearized Bethe-Salpeter equation

$$R_{\alpha\beta}(\omega) = R^0_{\alpha\beta}(\omega) + \sum_{\gamma\delta} R^0_{\alpha\gamma}(\omega)V^{ph}_{\gamma\delta}R_{\delta\beta}(\omega). \quad (5)$$

This method is usually referred to as a response-function formalism of the random-phase approximation to distinguish it from the more frequently used configuration-space formalism [41]. The reason we chose this formalism is because it is essential for an exact treatment of the continuum coupling.

1. The residual interaction

As explained in textbooks [42,43], the residual interaction $V^{ph}_{\alpha\beta}$ of Eq. (5) is connected to the static problem via the second

derivative of the energy functional

$$V^{ph}_{\alpha\beta} = \frac{\delta^2 E[\hat{\rho}]}{\delta\hat{\rho}_\alpha \delta\hat{\rho}_\beta}, \tag{6}$$

and hence, it depends on the same coupling constants $\alpha_i[\hat{\rho}]$ and their derivatives with respect to the densities. In this way, one ensures a fully self-consistent treatment of the dynamical problem. The point-coupling scheme allows one to write V^{ph} as a sum of separable terms, simplifying considerably the numerical solution of the Bethe-Salpeter equation. In particular, one can write

$$V^{ph}(1,2) = \sum_c \int_0^\infty dr\, Q^{(1)}_c(r) \upsilon_{cc'}(r) Q^{\dagger(2)}_{c'}(r), \tag{7}$$

where the upper indices (1) and (2) indicate that these operators act on the "coordinates" $1 = (r_1\Omega_1 s_1 d_1 t_1)$ and $2 = (r_2\Omega_2 s_2 d_2 t_2)$.

Each separable term is characterized by (c,r), the channel index c given by the discrete numbers $\{D, S, L, J, T\}$ and the radial mesh point r. In the point-coupling models under investigation, there are overall seven channels: one scalar S, three isoscalar V, and three isovector TV vectors. Assuming a coordinate mesh of 50 points, the final size of the interaction matrix is not larger than 350×350. The corresponding channel vertices $\hat{Q}^{(1)}_c(r)$ are local single-particle operators

$$\hat{Q}^{(1)}_c(r) = (-)^{S_c} \frac{\delta(r - r_1)}{r r_1} \hat{\Gamma}^{(1)}_c Y_L(\Omega_1). \tag{8}$$

Therefore, the Bethe-Salpeter [Eq. (5)] becomes

$$R_{cc'}(\omega) = R^0_{cc'}(\omega) + \sum_{c_1 c_2} R^0_{cc_1}(\omega) \upsilon_{c_1 c_2} R_{c_2 c'}(\omega), \tag{9}$$

which has the same formal solution as in Eq. (5). For the continuous variables of the channel index c, such as the radial coordinate r, Eq. (9) is an integral equation.

The interaction $\upsilon_{cc'}$ can be expressed as a matrix in the spin-isospin space, indicated by the index c. Apart from the direct terms $\alpha_i[\hat{\rho}]$ of the Lagrangian, $\upsilon_{cc'}$ also consists of the so-called rearrangement terms, as a result of the double variation of Eq. (6). Furthermore, the gradient term is described by the operator [23]

$$\Delta = r^2 \overleftarrow{\partial}_r \frac{1}{r^2} \overrightarrow{\partial}_r + \frac{L(L+1) - 2}{r^2}. \tag{10}$$

In Tables II and III, the exact form of the interaction matrices is displayed for the two parameter sets PC-F1 and DD-PC1. Further details can be found also in Refs. [23,44].

TABLE II. Structure of the matrix $\upsilon_{cc'}$ in spin-isospin space for the PC-F1 parametrization. The functional $F_i[\rho] = \alpha_i[\rho_i] + 2\alpha'_i[\rho_i]\rho_i + (1/2)\alpha''_i[\rho_i]\rho_i^2 + \delta_i\Delta$.

PC-F1	S	V	TV
S	$F_S[\rho_S]$	0	0
V	0	$F_V[\rho_V]$	0
TV	0	0	$F_{TV}[\rho_{TV}]$

TABLE III. Structure of the matrix $\upsilon_{cc'}$ for the DD-PC1 parametrization. The functional $F_V[\rho] = \{\alpha_V[\rho] + 2\alpha'_V[\rho]\rho + (1/2)\alpha''_V[\rho]\rho^2\} + (1/2)\alpha''_S[\rho]\rho_S^2 + (1/2)\alpha''_{TV}\rho_{TV}^2$.

DD-PC1	S	V	TV
S	$\alpha_S[\rho] + \delta_S\Delta$	$\alpha'_S[\rho]\rho_S$	0
V	$\alpha'_S[\rho]\rho_S$	$F_V[\rho]$	$\alpha'_{TV}[\rho]\rho_{TV}$
TV	0	$\alpha'_{TV}[\rho]\rho_{TV}$	$\alpha_{TV}[\rho]$

Apart from the Coulomb force

$$\upsilon_C(r,r') = \frac{4\pi e^2}{2L+1} \frac{r^L_<}{r^{L+1}_>}, \tag{11}$$

all other interaction terms are diagonal in r. Here, $r_<$ and $r_>$ are the smaller and the greater of r and r'. This force breaks isospin symmetry. Hence, one has to expand υ_C in its spin-isospin components:

$$\begin{aligned} V_C(1,2) &= \left(\frac{1}{2}(1+\tau_3)\right)^{(1)} \frac{e^2}{|\mathbf{r}_1 - \mathbf{r}_2|} \left(\frac{1}{2}(1+\tau_3)\right)^{(2)} \\ &= \frac{1}{4}\frac{e^2}{|\mathbf{r}_1 - \mathbf{r}_2|}(\mathbf{1}^{(1)}\mathbf{1}^{(2)} - \mathbf{1}^{(1)}\tau_3^{(2)} - \tau_3^{(1)}\mathbf{1}^{(2)} + \tau_3^{(1)}\tau_3^{(2)}). \end{aligned} \tag{12}$$

This means that in spin-isospin space, the Coulomb interaction can be split into four parts, but thankfully not into four additional channels. In particular, the two diagonal terms are added to the already existing isoscalar and isovector vector channels, while the other two correspond to off-diagonal terms. This leads to a Coulomb matrix $\upsilon^C_{cc'}(r,r')$ as shown in Table IV.

2. *The free response function*

The free response function $R^0_{cc'}(\omega)$ is the key point for a successful description of the RPA problem, since it includes all the microscopic properties of the nucleus under investigation. In the discrete quasiparticle space, i.e., in the spectral representation, it can be written as

$$\begin{aligned} \mathcal{R}^0_{2qp} = \sum_{\alpha\leqslant\beta}^{E^{\max}_{ph}} \frac{1}{1+\delta_{\alpha\beta}} \eta^S_{\alpha\beta} \langle\alpha||Q^\dagger_c||\beta\rangle_r \eta^{S'}_{\alpha\beta} \langle\alpha||Q_{c'}||\beta\rangle_{r'} \\ \times \left(\frac{1}{\omega - E_{\alpha\beta} + i\eta} - \frac{1}{\omega + E_{\alpha\beta} + i\eta}\right), \end{aligned} \tag{13}$$

where the indices α and β refer to the two-quasiparticle states in the excitation, while $|\alpha\rangle_r = |\alpha(r)\rangle$ and $|\beta(r)\rangle$ are the corresponding radial single-particle wave functions. The

TABLE IV. Structure of the channel matrix $\upsilon^C_{cc'}$ for the Coulomb interaction.

	S	V	TV
S	0	0	0
V	0	$\frac{1}{4}\upsilon_C$	$-\frac{1}{4}\upsilon_C$
TV	0	$-\frac{1}{4}\upsilon_C$	$\frac{1}{4}\upsilon_C$

factors $\eta^c_{\alpha\beta} = u_\alpha v_\beta + (-)^{S_c} u_\alpha v_\beta$ include the BCS occupations u_α and v_α. The energy $E_{\alpha\beta} = E_\alpha + E_\beta$ is the sum of two quasiparticle energies. In addition, the smearing parameter η is used in Eq. (13) in order to avoid a divergence of the free response function, and its value is often adjusted to the observed width of the giant resonances. It has to be emphasized that according to the no-sea approximation in the relativistic RPA the sum in Eq. (13) includes also transitions to negative energy solutions [41,45] since the vacuum polarization is neglected.

One of the important questions which arises by using the spectral representation of Eq. (13) is the question of completeness of the basis. Numerical limitations require a basis truncation, which can play a role in the final solution. In practical calculations, an energy cutoff $E^{ph}_{\rm cut} = 500$ MeV for the particles and a corresponding $E^{ah}_{\rm cut} = -2000$ MeV for the antiparticles is required to achieve a converged solution. This fact, combined with the additional excitations to the antiparticle states, leads to a very large configuration space [41].

In continuum QRPA, however, the situation is very different. Here, one makes use of the nonspectral representation of the free response function, which is given by

$$\mathcal{R}^0_{cc'} = \sum_\alpha u^2_\alpha \langle\alpha(r)|\hat{Q}^\dagger_c g_{\kappa_\alpha}(\omega+\varepsilon_\alpha)\hat{Q}_{c'}|\alpha(r')\rangle + \langle\alpha(r)|\hat{Q}^\dagger_{c'} g_{\kappa_\alpha}(-\omega+\varepsilon_\alpha)\hat{Q}_c|\alpha(r')|\rangle, \quad (14)$$

where the relativistic Green function is

$$g_\kappa(E) = \begin{cases} |w_\kappa(r)\rangle\langle u^*_\kappa(r')|/W & \text{for} \quad r > r', \\ |u_\kappa(r)\rangle\langle w^*_\kappa(r')|/W & \text{for} \quad r < r'. \end{cases} \quad (15)$$

The two-dimensional spinors

$$|u_\kappa(r)\rangle = \begin{pmatrix} f_u(r) \\ i g_u(r) \end{pmatrix}$$

and

$$|w_\kappa(r)\rangle = \begin{pmatrix} f_w(r) \\ i g_w(r) \end{pmatrix}$$

are the regular and the irregular wave functions of a continuum state with the quantum number $\kappa = (lj)$ and the energy E. Further details are given in Ref. [23]. Since $|w_\kappa(r)\rangle$ behaves as an outgoing wave as $r \to \infty$, it is a complex quantity. In this way, the strength function in Eq. (4) has a nonvanishing imaginary part without the need of any smearing parameter, as in Eq. (13). The denominator W describes the Wronskian of the system,

$$W = \langle w_\kappa(r)|u^*_\kappa(r)\rangle = f_w(r)g_u(r) - g_w(r)f_u(r), \quad (16)$$

and is independent of r. In the particular case where the energy of the continuum state meets the value of an eigenstate $E = \omega + \varepsilon_\alpha = \varepsilon_p$, the two wave functions $|u_\kappa\rangle$ and $|w_\kappa\rangle$ become identical and the Green function diverges, similar to the case in Eq. (13). So, the two expressions of the free response functions in Eqs. (13) and (14) are in principle identical, but in practice and due to the space truncation of the spectral representation, differences are expected.

Consequently, one of the big advantages of the nonspectral or continuum representation [Eq. (14)] is the inclusion of the entire configuration space, without the need of any truncation technique. This is achieved by summing over blocks of well-defined quantum numbers κ. The wave functions are exact and obey the proper boundaries at infinity. In this way, the numerical effort can be reduced by more than one order of magnitude, as compared to the conventional RRPA approaches, where the continuum is discretized [37]. Finally, as far as the solution is concerned, the inclusion of the full space ensures a more realistic description of the nuclear collective properties and better agreement with the experimental data [23].

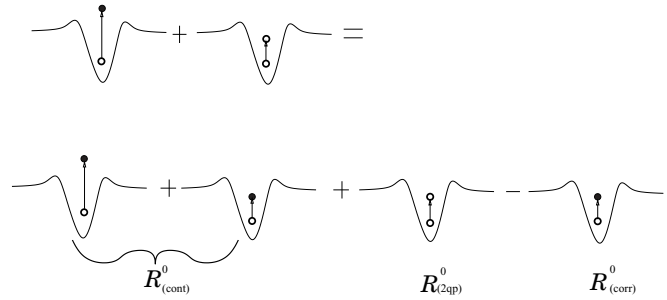

FIG. 1. Various configurations used for the calculation of the free quasiparticle response. Filled circles (•) refer to a pure particle ($v^2_k = 0$), while empty circles (○) indicate quasiparticles ($v^2_k > 0$). Details are given in the text.

Despite its simplicity, a problem arises when pairing correlations are included. From Eq. (14), we see that all levels lying in the continuum have $u_\beta = 1$, i.e., they are all considered as pure particles. But this is not the case in the QRPA model, where levels close to the Fermi surface (some of them above the single-particle continuum limit) must be treated as quasiparticles. That implies that in order to be consistent, we need to modify the continuum representation to properly account for the states within the space, where pairing is active.

In Fig. 1, we schematically illustrate our technique, which has been used in the past to define the continuum QRPA in nonrelativistic models [9,10]. In this figure, the allowed transitions are displayed as a sum of three different terms. At first, the continuum term $\mathcal{R}^0_{\rm cont}$ of Eq. (14) includes the transitions to the entire single-particle space.

The two-quasiparticle excitations within the pairing active space are treated by the two-quasiparticle response function Eq. (13) up to the pairing cutoff, which does not exceed the $E_p = +20$ MeV.

However, in order to avoid double counting of the excitations in the active pairing space, one needs to subtract a correction term, which describes transitions from a quasiparticle to a pure particle using the expression

$$\mathcal{R}^0_{\rm corr} = \sum_{\alpha\leqslant\beta}^{E_p} \frac{1}{1+\delta_{\alpha\beta}} \langle\alpha||Q^\dagger_c||\beta\rangle_r \langle\alpha||Q_{c'}||\beta\rangle_{r'} \times \left\{ \frac{v^2_\alpha}{\omega - \Omega_{\alpha,\beta} + i\eta} - \frac{v^2_\alpha}{\omega + \Omega_{\alpha,\beta} + i\eta} + \frac{v^2_\beta}{\omega - \Omega_{\beta,\alpha} + i\eta} - \frac{v^2_\beta}{\omega + \Omega_{\beta,\alpha} + i\eta} \right\}, \quad (17)$$

where $\Omega_{\alpha,\beta} = E_\beta + \varepsilon_\alpha - \lambda$. The indices α and β run only over the partially occupied states below the continuum limit ($\varepsilon_\alpha < 0$). Consequently, a proper treatment of the quasiparticle CRPA requires that the response function

$$\mathcal{R}^0(r, r'\,\omega) = \mathcal{R}^0_{\rm cont}(r, r'\,\omega) + \mathcal{R}^0_{\rm 2qp}(r, r'\,\omega) - \mathcal{R}^0_{\rm corr}(r, r'\,\omega) \tag{18}$$

is used in Eq. (5).

It has to be emphasized that all the particle states above the pairing window as well as the states in the Dirac sea do not participate in the above calculation, since they are completely taken into account in the continuum part $\mathcal{R}^0_{\rm cont}(r, r'\,\omega)$ in an exact way.

III. RESULTS AND DISCUSSIONS

In this section, we show the IVGDR results for various spherical open-shell nuclei, using both the continuum and the discrete QRPA models.

As a first step, the ground state of the nucleus is determined by solving the self-consistent RMF equations for the parameter sets PC-F1 and DD-PC1 given in Table I. Pairing correlations are treated within the BCS model with a constant gap. For the pairing gap, either the empirical expression $\Delta_{n,p} = 12.0/\sqrt{A}$ or the gaps deduced from nuclear mass tables [47] can be used, with the difference to be insignificant to the final outcome.

Using the single-particle wave functions and the corresponding quasiparticle energies of this static solution, we determine the free response $\mathcal{R}^0$ of Eq. (18). Finally, we solve the Bethe-Salpeter Eq. (9) to get the strength distribution $S(\omega)$.

At the same time, we perform similar calculations using the conventional RPA approach, where the continuum is fully discretized. For those calculations, we have used an energy cutoff $|\epsilon_p - \epsilon_h| < E^{ph}_{\rm cut} = 300$ MeV for the configurations with particles above the Fermi sea and $|\epsilon_a - \epsilon_h| < E^{ah}_{\rm cut} = 2000$ MeV for configurations with anti-particles in the Dirac sea.

In the left panel of Fig. 2, we show the cross section for the IVGDR in the open-shell nucleus ^{124}Sn for the two parameter sets PC-F1 (red solid line) and DD-PC1 (blue dashed line), as well as the experimental values from Ref. [46]. The cross section is linear to the $E1$ strength of Eq. (4) according to

$$\begin{aligned}\sigma(E) &= \frac{16\pi^3 e^2}{9\hbar\, c} E\, S(E)\ \text{fm}^2 \\ &= 4.022\, E\, S(E)\ \text{mb}.\end{aligned} \tag{19}$$

The two parametrizations PC-F1 and DD-PC1 perform very well in reproducing the giant-dipole resonance, as compared to experimental data [46]. The energy-weighted sum rule for the two forces are found at $m_1 = 2043.47$ and $m_1 = 2151.85$ mb MeV, respectively. These results are in agreement with results of the discrete QRPA and, as usual, somewhat (13.7% and 19.7%) larger than those obtained from the classical Thomas-Reiche-Kuhn (TRK) sum rule

$$m_{\rm TRK} = 60.0\frac{NZ}{A} = 1782.32\ \text{mb MeV}. \tag{20}$$

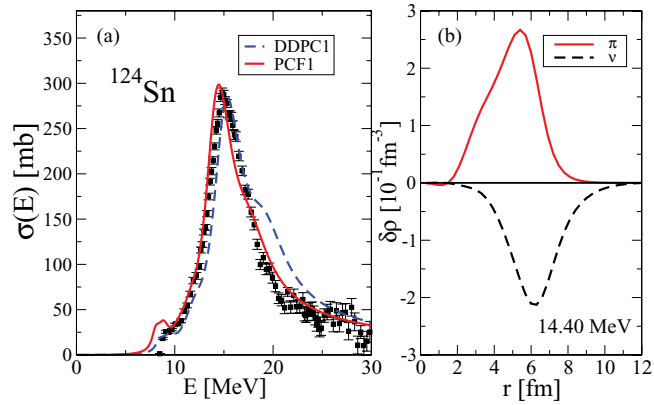

FIG. 2. (Color online) (a) IVGDR strength distributions for ^{124}Sn using the forces PC-F1 (red solid line) and DD-PC1 (blue dashed line). The experimental results are taken from Ref. [46]. (b) Neutron and proton transition densities for the GDR at $E = 14.40$ MeV.

Because of the exact coupling to the continuum, the escape width $\Gamma^\uparrow$ of the IVGDR is automatically taken into account. However, in heavy nuclei, $\Gamma^\uparrow$ is very small, due to the high Coulomb and centrifugal barriers, which prevent the excited nucleon from escaping. The rest of the total width comes mainly from the coupling to more complex configurations ($2ph$, $3ph$, etc.). Here, this part is treated approximately by an additional smearing parameter, which can be energy or temperature dependent [48], according to the expression

$$\Gamma(E) = \Gamma_0 \frac{E^2 + 4\pi^2 T^2}{E^2_{\rm GDR}}. \tag{21}$$

In our study, we have calculated the width by using $\Gamma_0 = 1.4$ MeV and $T = 0$. In the right panel of Fig. 2, we give the proton and neutron transition densities $\delta\rho(r)$ associated with the GDR peak at $E = 14.40$ MeV. We see that the excitation at this energy has a pure isovector character, since the neutrons are coherently oscillating against the protons.

In Fig. 3, the centroid energies of the IVGDR are revealed for several Sn isotopes, which have been well identified experimentally [1,46,49]. The centroid energy $\bar{E} = m_1/m_0$ is calculated in the same energy window as the one used in the experimental analysis, i.e., between 13 and 18 MeV. It can be clearly seen that both discrete and continuum QRPA approaches predict a similar decrease of the centroid energies with respect to the mass number of the isotope, but the agreement with the experimental data is better reproduced with the continuum approach.

In Table V, results for the two density functionals PC-F1 and DD-PC1 are compared using the continuum approach. We have studied a series of stable spherical nuclei, which have experimentally well-defined collective properties. It appears that the force PC-F1 is, in general, slightly better in performance, although both sets are very successful in predicting the collective properties.

As it is, for instance, clearly seen in Fig. 2, in the case of neutron-rich nuclei, in addition to the giant-dipole resonance, a small peak appears at the energy region of the neutron emission threshold around $E \sim 8$ MeV. This pygmy mode is classically

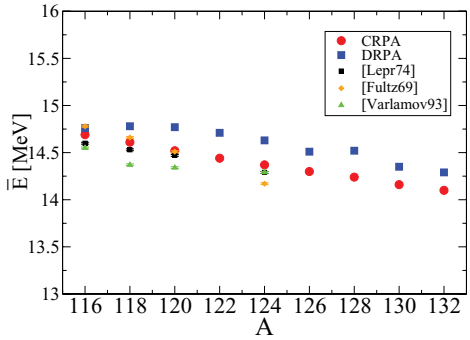

FIG. 3. (Color online) Centroid energies for several Sn isotopes using the discretized RPA (DRPA) (blue boxes) and the CRPA (red circles) approaches. The experimental results are deduced from Refs. [1,46,49].

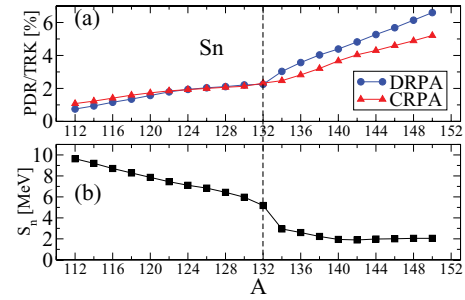

FIG. 4. (Color online) (a)Ratio of the PDR strength to the TRK sum rule for various Sn isotopes. The blue circles indicate discrete RPA results, while the red triangles are continuum RPA results. The calculated PDR is integrated up to 11 MeV. In both cases, the force PC-F1 has been used. (b) Neutron emission threshold for the same range of Sn isotopes. Here the force PC-F1 is used.

interpreted as an oscillation of the neutron skin against the isospin-saturated proton-neutron core, and it seems to have a collective character as well.

The collectiveness of this pygmy mode can be studied by plotting the evolution of its strength with respect to the mass number. As we show in the upper panel of Fig. 4, the contribution of the pygmy-dipole resonance (PDR) strength to the Thomas-Reiche-Kuhn sum rule increases considerably as we move to heavier isotopes, meaning that all the additional neutrons participate in this resonance. In particular, we find that there is a sharper increase after the doubly magic isotope ^{132}Sn, which is observed in both the continuum and the discrete approach. This can be connected to the sharp decrease of the particle emission threshold at exactly the same isotope, as we see in the lower panel of Fig. 4.

A more careful study in this low-lying mode has shown that its determination is not easy for two main reasons. First, the experimental identification is very difficult in this area, since it often lies below the particle emission threshold, where (γ,n) reactions are no more possible. The other reason is that

TABLE V. Excitation energy of the isovector dipole resonance for several nuclei, using both DD-PC1 and PC-F1 self-consistent interactions. The centroid energies have been calculated in the area 11–18 MeV.

		DD-PC1	PC-F1	Expt. [MeV]	Ref.
^{70}Zn	E_0	17.50	16.70	17.25 ± 0.08	[50]
	$\bar{E}$	16.00	15.86	15.68 ± 0.02	
^{94}Zr	E_0	16.60	15.60	16.67 ± 0.07	[51]
	$\bar{E}$	15.90	15.58	16.00 ± 0.01	
^{124}Sn	E_0	15.40	14.40	14.67 ± 0.08	[1]
	$\bar{E}$	14.99	14.70	14.34 ± 0.02	
^{130}Te	E_0	15.30	14.60	14.53 ± 0.13	[52]
	$\bar{E}$	14.96	14.66	14.27 ± 0.01	
^{138}Ba	E_0	15.20	14.40	15.29 ± 0.15	[53]
	$\bar{E}$	14.89	14.55	14.64 ± 0.01	
^{144}Sm	E_0	15.10	14.50	15.37 ± 0.13	[54]
	$\bar{E}$	15.39	14.58	14.77 ± 0.02	
^{208}Pb	E_0	13.60	12.80	13.50 ± 0.19	[55]
	$\bar{E}$	14.13	13.78	13.52 ± 0.04	

the exact position of this soft mode has been found to be very sensitive to the basis truncation, i.e., to the choice of the energy cutoff $E_{\rm cut}^{ph}$. This can be clearly seen in Fig. 5, where we compare the $E1$ strength of ^{124}Sn derived from the discrete RPA approach with various energy cutoffs with results from continuum RPA. For the sake of the present discussion, a very small smearing parameter Γ has been used. It is very interesting to see how the position of the pygmy mode moves to lower energies as we increase the configuration space, and also that it approaches the position of the continuum RPA, in which the entire configuration space is included.

Therefore, it becomes evident that a proper treatment of the continuum seems to be very important in the calculation of the low-lying collective phenomena. It has to be emphasized that till now in all the previous relativistic investigations, this has not been possible. In Fig. 6, we go further and show the details of the PDR in the isotope ^{132}Sn, which has only recently been identified experimentally [56].

In the left panel of Fig. 6, the blue dashed line corresponds to the discrete RPA, while the red solid one shows the continuum RPA calculations. Although the experimental uncertainties are still large in this neutron-rich nucleus, we find a nice agreement with the relativistic-RPA model, in particular, in the continuum approach. In the right panel of

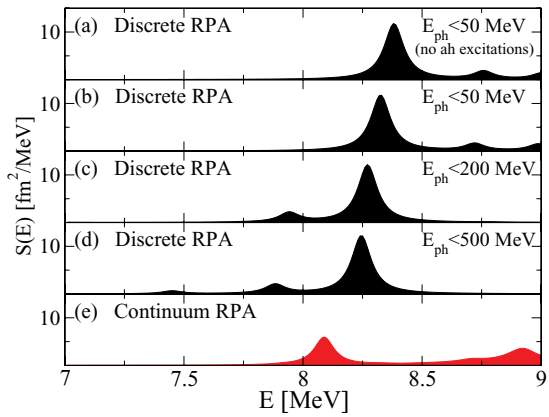

FIG. 5. (Color online) PDR strength using DRPA with different energy cutoffs [(a)–(d)] and CRPA (e).

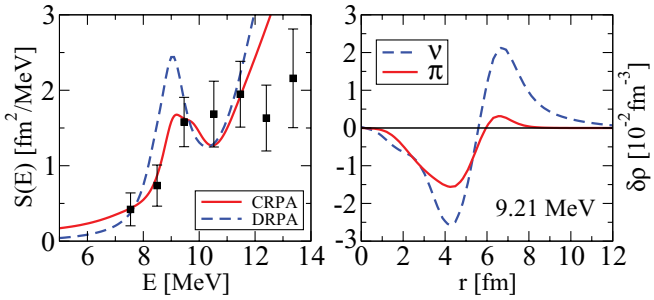

FIG. 6. Panel (a): The low-lying $E1$ strength distributions for ^{132}Sn using Discrete (blue dashed line) and Continuum RPA (red solid line). In both cases, the point-coupling force PC-F1 has been applied. Panel (b): The proton and neutron transition densities at the peak of the soft mode. The experimental data are taken from Ref. [56].

Fig. 6, the proton and neutron transition densities at the peak energy are used to show the pygmy character of this mode, i.e., the oscillation of a relatively pure neutron skin against the isospin-saturated proton-neutron core.

IV. CONCLUSIONS

Starting from a point-coupling Lagrangian, we have used the relativistic continuum QRPA approach to examine the $E1$ collective excitation spectra of spherical open-shell nuclei. This nonspectral method has several advantages. The use of exact scattering wave functions with proper boundary conditions instead of expansions in a harmonic oscillator basis in the continuum allows for the simultaneous inclusion of the entire continuum and the contributions of the Dirac sea. Furthermore, large sums over unbound states are avoided, which is extremely important in relativistic model, since the unbound states in the Dirac sea are the root for computationally very expensive calculations.

In these investigations the ground-state properties are calculated using a relativistic point-coupling Lagrangian with the parameter sets PC-F1 and DD-PC1. The RMF equations are solved in r space self-consistently. For open-shell nuclei, the BCS model is applied to treat the pairing correlations properly.

The residual particle-hole interaction used in the QRPA calculations is derived from the same parameter sets as the second derivative of the energy functional with respect to the density. In this way, no additional parameter is required for the study of the dynamical problem. One has current conservation and an exact separation of the spurious modes, and one is able to reproduce the collective properties, as for instance, the giant-multipole resonances, in a fully self-consistent way.

The calculations are carried out by using two different point-coupling forces, namely the PC-F1 and DD-PC1. The interaction then includes the basic zero range terms, rearrangement terms due to density dependence, the derivative terms which simulate the finite range of the nuclear interaction, the various current-current terms, and finally, the Coulomb interaction between protons.

We have used the continuum QRPA approach to study collective properties, which are initiated by photo-absorption processes. We have shown that the model performs well in describing both the giant-dipole and the soft-pygmy resonance. In particular, although there are not large differences in the details between the continuum and the discrete RPA calculations as far as the GDR is concerned, there is still some systematic difference close to the neutron separation threshold of stable nuclei and an even larger one for the extreme neutron-rich nuclei. New (γ,γ') experiments on this low-lying area [57] are expected to be of paramount importance to the understanding of the real contribution of the exact coupling to the continuum.

Finally, this approach accounts for nuclei far from the drip lines where no level in the continuum is occupied, and thus the BCS models can be safely applied. For nuclei up to the drip line, the relativistic Hartree-Bogoliubov approximation would be required. Investigations in this direction are in progress.

ACKNOWLEDGMENTS

Helpful discussions with S. Goriely, G. Lalazissis, D. Pena Arteaga, T. Nikšić, and D. Vretenar are gratefully acknowledged. This work was financially supported by the FNRS (Belgium) and the Communauté française de Belgique (Actions de Recherche Concertées) and by the DFG Cluster of Excellence "Origin and Structure of the Universe" (www.universe-cluster.de).

[1] A. Lepretre, H. Beil, R. Bergere, P. Carlos, A. D. Miniac, A. Veyssiere, and K. Kernbach, Nucl. Phys. A **219**, 39 (1974).
[2] S. Shlomo and G. F. Bertsch, Nucl. Phys. A **243**, 507 (1975).
[3] R. H. Lemmer and M. Veneroni, Phys. Rev. **170**, 883 (1968).
[4] K. Dietrich and K. Hara, Nucl. Phys. A **111**, 392 (1968).
[5] K. Dietrich and C. Dover, Nucl. Phys. A **135**, 481 (1969).
[6] G. F. Bertsch and S. F. Tsai, Phys. Rep. **18**, 125 (1975).
[7] S. F. Tsai, Phys. Rev. C **17**, 1862 (1978).
[8] T. Udagawa and B. T. Kim, Phys. Rev. C **40**, 2271 (1989).
[9] S. Kamerdzhiev, R. J. Liotta, E. Litvinova, and V. I. Tselyaev, Phys. Rev. C **58**, 172 (1998).
[10] K. Hagino and H. Sagawa, Nucl. Phys. A **695**, 82 (2001).
[11] M. Matsuo, Nucl. Phys. A **696**, 371 (2001).
[12] M. Matsuo, Prog. Theor. Phys. Suppl. **146**, 110 (2002).
[13] E. Khan, N. Sandulescu, M. Grasso, and N. V. Giai, Phys. Rev. C **66**, 024309 (2002).
[14] I. N. Borzov, Phys. Rev. C **67**, 025802 (2003).
[15] T. Nakatsukasa and K. Yabana, Phys. Rev. C **71**, 024301 (2005).
[16] K. Yoshida, M. Yamagami, and K. Matsuyanagi, Nucl. Phys. A **779**, 99 (2006).
[17] H. Oba and M. Matsuo, Phys. Rev. C **80**, 024301 (2009).
[18] K. Mizuyama, M. Matsuo, and Y. Serizawa, Phys. Rev. C **79**, 024313 (2009).
[19] K. Wehrberger and F. Beck, Phys. Rev. C **37**, 1148 (1988).
[20] C. J. Horowitz and J. Piekarewicz, Nucl. Phys. A **511**, 461 (1990).

[21] J. R. Shepard, E. Rost, and J. A. McNeil, Phys. Rev. C **40**, 2320 (1989).
[22] J. Piekarewicz, Phys. Rev. C **62**, 051304(R) (2000).
[23] J. Daoutidis and P. Ring, Phys. Rev. C **80**, 024309 (2009).
[24] N. Paar, D. Vretenar, E. Khan, and G. Coló, Rep. Prog. Phys. **70**, 691 (2007).
[25] S. Goriely and E. Khan, Nucl. Phys. A **706**, 217 (2002).
[26] A. Bulgac, arXiv:nucl-th/9907088.
[27] J. Dobaczewski, H. Flocard, and J. Treiner, Nucl. Phys. A **422**, 103 (1984).
[28] T. Gonzales-Llarena, J. L. Egido, G. A. Lalazissis, and P. Ring, Phys. Lett. B **379**, 13 (1996).
[29] M. Serra and P. Ring, Phys. Rev. C **65**, 064324 (2002).
[30] D. Vretenar, A. V. Afanasjev, G. A. Lalazissis, and P. Ring, Phys. Rep. **409**, 101 (2005).
[31] J. D. Walecka, Ann. Phys. (NY) **83**, 491 (1974).
[32] P. Manakos and T. Mannel, Z. Phys. A **334**, 481 (1989).
[33] T. Hoch, D. Madland, P. Manakos, T. Mannel, B. Nikolaus, and D. Strottman, Phys. Rep. **242**, 253 (1994).
[34] Y. Nambu and G. Jona-Lasinio, Phys. Rev. **122**, 345 (1961).
[35] T. Bürvenich, D. G. Madland, J. A. Maruhn, and P.-G. Reinhard, Phys. Rev. C **65**, 044308 (2002).
[36] T. Nikšić, D. Vretenar, and P. Ring, Phys. Rev. C **78**, 034318 (2008).
[37] T. Nikšić, D. Vretenar, and P. Ring, Phys. Rev. C **72**, 014312 (2005).
[38] G. A. Lalazissis, S. Karatzikos, R. Fossion, D. Peña Arteaga, A. V. Afanasjev, and P. Ring, Phys. Lett. B **671**, 36 (2009).
[39] G. A. Lalazissis, T. Nikšić, D. Vretenar, and P. Ring, Phys. Rev. C **71**, 024312 (2005).
[40] J. Daoutidis and G. A. Lalazissis, J. Phys. G **31**, 659 (2005).
[41] P. Ring, Z.-Y. Ma, N. Van Giai, D. Vretenar, A. Wandelt, and L.-G. Cao, Nucl. Phys. A **694**, 249 (2001).
[42] P. Ring and P. Schuck, *The Nuclear Many-Body Problem* (Springer-Verlag, Berlin, 1980).
[43] M. A. L. Marques, C. A. Ullrich, F. Nogueira, A. Rubio, K. Burke, and E. G. U. Gross (eds.), *Time-Dependent Density Functional Theory* (Springer, Heidelberg, 2006).
[44] J. K. Daoutidis, Ph.D. thesis, Technical University of Munich, 2009.
[45] J. F. Dawson and R. J. Furnstahl, Phys. Rev. C **42**, 2009 (1990).
[46] S. C. Fultz, B. L. Berman, J. T. Caldwell, R. L. Bramblett, and M. A. Kelly, Phys. Rev. **186**, 1255 (1969).
[47] S. Goriely, N. Chamel, and J. M. Pearson, Phys. Rev. C **82**, 035804 (2010).
[48] E. Betak, J. Kopecky, and F. Cvelbar, Phys. Rev. C **46**, 945 (1992).
[49] V. V. Varlamov, Yad. Konst. **1**, 52 (1993).
[50] A. Goryachev and G. Zalesnyy, Vopr. Teor. Yad. Fiz. 8121 (1982).
[51] B. L. Berman, J. T. Caldwell, R. R. Harvey, M. A. Kelly, R. L. Bramblett, and S. C. Fultz, Phys. Rev. **162**, 1098 (1967).
[52] A. Lepretre, H. Beil, R. Bergere, P. Carlos, J. Fagot, A. Miniac, A. Veyssiere, and H. Miyase, Nucl. Phys. A **258**, 350 (1976).
[53] B. Berman, S. Fultz, J. Caldwell, M. Kelly, and S. Dietrich, Phys. Rev. C **2**, 2318 (1970).
[54] P. Carlos, H. Beil, R. Bergere, A. Lepretre, A. de Minac, and A. Veyssiere, Nucl. Phys. A **159**, 561 (1970).
[55] A. Veyssiere, H. Beil, R. Bergere, P. Carlos, and A. Lepretre, Nucl. Phys. A **159**, 561 (1970).
[56] P. Adrich, A. Klimkiewicz, M. Fallot, K. Boretzky, T. Aumann, D. Cortina-Gil, U. D. Pramanik, T. W. Elze, H. Emling, H. Geissel, M. Hellström, K. L. Jones, J. Kratz, R. Kulessa, Y. Leifels, C. Nociforo, R. Palit, H. Simon, G. Surówka, K. Sümmerer, and W. Walus, Phys. Rev. Lett. **95**, 132501 (2005).
[57] H. K. Toft, A. C. Larsen, U. Agvaanluvsan, A. Burger, M. Guttormsen, G. E. Mitchell, H. T. Nyhus, A. Schiller, S. Siem, N. U. H. Syed, and A. Voinov, Phys. Rev. C **81**, 064311 (2010).